Journal of Magnetism and Magnetic Materials 38 (1983) 1–22
North-Holland

MAGNETO-OPTICAL PROPERTIES OF METALLIC FERROMAGNETIC MATERIALS

K.H.J. BUSCHOW, P.G. van ENGEN and R. JONGEBREUR

Philips Research Laboratories, 5600 JA Eindhoven, The Netherlands

Received 17 March 1983

The authors have studied the magneto-optical Kerr rotation in more than 200 metallic systems comprising alloys as well as intermetallic compounds of 3d transition metals. For all these materials the crystal structure, the lattice constants, the room temperature magnetization and the room temperature Kerr rotation at two different wavelengths are specified. For several series of ternary compounds, comprising Heusler alloys Ni_2In-type compounds and $Cr_{23}C_6$ type compounds, we determined the saturation moment at 4.2 K. For a number of representative alloys or compounds a study was also made of the wavelength dependence of the complex polar Kerr effect. The values of the Kerr rotation obtained at 633 nm were compared with the corresponding values of the measured magnetization. Systematic trends were observed and have been used to classify metallic systems into systems where the Kerr rotation will not reach values much in excess of 1° and systems where higher values are likely to be found.

1. Introduction

The magneto-optical properties of magnetic materials are of considerable interest since it has been demonstrated that crystalline [1–3] as well as amorphous materials [4–7] exist that can be applied in thermomagnetic recording media. The stored information can be read by using either the Faraday- or the Kerr effect. In both cases sufficiently high signal-to-noise ratios can only be obtained in materials in which these effects are relatively large. Although the performance of magneto-optical storage materials based on amorphous rare earth–transition metal films are quite satisfactory [6,7] there is still a need to find materials that have a larger Kerr rotation, particularly for such applications as video recording.

It is clear that, apart from a strong Kerr effect, the magnetic properties have to meet several other requirements to make a given material suitable for use as a magneto-optical recording medium. One of these requirements is the presence of a positive uniaxial anisotropy which, in spite of the demagnetization field can keep the magnetization perpendicular to the film plane. Further requirements are a compensation temperature or Curie temperature not too far above room temperature or a coercive force decreasing rapidly with temperature. In the present study we will disregard all these requirements and focus our attention exclusively on the Kerr rotation of the various materials. The reason for this is that there is a general lack of information on the magneto-optical properties of magnetic metallic systems (although the magnetic properties are well known). Furthermore, no simple models seem to exist that relate these properties to other physical properties, even in the case of the few materials for which experimental magneto-optical data are available (see for instance refs. [1–3] and papers cited in these reviews). In other words, there is no such a thing as a "rule of thumb" that could be used in the search for new materials having a large Kerr rotation. The implication of the latter statement will be clear. The results of the present study are necessarily a "poor man's approach" to the problem: We have prepared all alloys and intermetallics that are known from the literature to be ferro- or ferrimagnetic above room temperature and have measured their Kerr rotation and their room temperature magnetization. In cases were the alloys or intermetallics form part of a series whose members

0304-8853/83/0000–0000/$03.00

have similar physical properties we have restricted our measurements to representative members of such series.

2. Experimental

2.1. Sample preparation

Most of the crystalline samples investigated were prepared by arc melting in an atmosphere of purified argon gas. Whenever X-ray diffraction showed that a sample was not single-phase after arc-melting, vacuum annealing was applied. For this purpose the sample was wrapped in Ta foil and sealed into an evacuated quartz tube. The annealing time and the annealing temperature are different for each sample and are stated separately in the list of materials given below. In some cases single-phase samples could only be obtained by quenching them in water after vacuum annealing. This is indicated in the tables by means of the symbol q. Lattice constants were derived from X-ray diagrams obtained by means of CuK_α radiation. For the magneto-optical measurements a flat portion of the sample was polished with diamond paste.

2.2. Kerr effect measurements

In general, the polar Kerr rotation was measured at two wavelengths using a HeNe laser (wavelength $\lambda = 633$ nm) and a solid-state GaAs laser ($\lambda = 830$ nm). The angle of incidence on the sample was smaller than 0.3° and a maximum magnetic field of 1280 kA/m (16 kOe) was applied. The wave-length dependence of the Kerr rotation φ_K and of the Kerr ellipticity ϵ_K was studied on only a few representative samples, using a second experimentally set-up with a Xe-arc light source and a monochromator. Here the mean angle of incidence was smaller than 4.5° and the maximum magnetic field amounted to 960 kA/m. Photon energies ranged from 0.6 to 4.4 eV. In both set-ups a Faraday modulator was used for polarization modulation. During the wavelength dependent measurements samples with a relatively high magnetization ($\sigma > 120$ Am^2kg^{-1} were not always saturated owing to the high demagnetizing fields. Comparison of the $2\varphi_K$ values listed for the two wavelengths in the tables with the corresponding $2\varphi_K$ values shown in the spectra shows that the error is small and will not affect the discussion of the Kerr spectra.

2.3. Magnetic measurements

Since it was the purpose of the present investigation to compare the polar Kerr rotation with the corresponding magnetization we restricted the magnetic measurements mainly to room temperature. Saturation moments at 4.2 K were determined only in relatively few cases. The magnetic measurements were performed on a PAR vibrating sample magnetometer. Magnetic isotherms were recorded on powdered polycrystalline samples with field strengths up to 1440 kA/m (18 kOe). As the magnetization of most of the compounds and alloys investigated became saturated in fields of a few hundred of kA/m, the value of the magnetization (σ) measured at 1440 kA/m is therefore well suited for comparison with the corresponding values of the Kerr rotation ($2\varphi_K$).

3. Experimental results

The results will be presented in two different forms. Numerical results for all the materials investigated have been collected in tables 1–12. As is customary, we have represented the formula composition of intermetallic compounds of the elements A and B by means of A_nB_m where n and m are small integers. In those cases where the alloy or compound is a representative within a series of solid solutions the formula composition is indicated by means of $A_{1-x}B_x$, where $1-x$ and x add up to 100%. In a few cases our method of sample preparation resulted in an alloy or compound slightly different from that expected on the basis of published phase diagram data (see refs. [8–10]). In order to properly specify the nature of the samples on which our magneto-optical ($2\varphi_K$) and magnetic measurements (σ) were made we have included in the tables crystal structure and lattice constants determined from our X-ray diagrams. The reduced Kerr rotation, defined by means of the ratio $2\varphi_K/\sigma$ is listed in the tables (for $\lambda = 633$

nm only). It gives an impression of the extent to which the Kerr rotation is correlated with the corresponding magnetization.

Several of the results have also been represented in graphical form. Here we have restricted ourselves to cases where the number of ferromagnetic alloys or compounds in a given binary system is sufficiently large or extends over a sufficiently large concentration interval to make plotting of the concentration dependence of $2\varphi_K$ and σ meaningful.

3.1. Ni-base materials

Compared to the large number of ferromagnetic alloys or compounds based on Fe or Co the number of ferromagnetic alloys or compounds based on Ni or Mn is relatively small. In the case of Ni this is due to the smallness of the Ni moment. The Ni 3d band being nearly filled, further band filling or band broadening resulting from alloying or compounding leads to a collapse of the 3d moment. As can be derived from the third column in table 1, all the materials listed are alloys of the α-Ni solid solution range in the binary phase diagrams. The binary Ni compounds in the corresponding binary systems are not ferromagnetic above room temperature. It can be seen from the results listed in table 1 that alloying of Ni with non-magnetic elements leads to a decrease of the Kerr rotation, the only exception being Pt.

The Kerr spectra of several alloys in which Ni has been combined with s, p metals or with Cu are compared with the spectrum of Ni in fig. 1. For practical reasons we have plotted only the energy dependence of the Kerr rotation $2\varphi_K$. The energy dependence of the ellipticity $2\epsilon_K$ is only shown for the Sn alloy, as an example. It can be seen from fig. 1 that the main features of the Kerr rotation spectra in Ni are preserved upon alloying, although there is a substantial reduction of the intensity of the spectra when Ni is combined with Al, in Sn. There are only subtle shifts in the first maximum of $\varphi_K(E)$ at 1.5 eV and the same holds with respect to the energy (at about 0.9 eV) at which $\varphi_K(E)$ shows a sign reversal. On the other hand, alloying with Al, In and Sn has a marked influence on the second $\varphi_K(E)$ maximum near 3 eV. The amplitude of φ_K associated with the second maximum has decreased relatively to that of the first maximum. The location of this maximum is seen to shift to lower energies and the same

Table 1
Crystalchemical, magnetic and magneto-optic data of several Ni alloys. The magnetization (σ) and polar Kerr rotation angle ($2\varphi_K$) were measured at room temperature in a field of 1280 kA/m

Alloy or compound	Heat treatment	Crystal structure	Lattice a (Å)	σ (Am^2kg^{-1})	$2\varphi_K$(deg)		$\frac{2\lvert\varphi_K\rvert}{\sigma}\times10^3$
					633 nm	830 nm	
Ni	as-cast	fcc (A_1)	3.524	55	−0.26	−0.29	4.7
$Ni_{92}Cu_8$	2w 1000 (g)	fcc (A_1)	3.526	45	−0.19	−0.21	4.2
$Ni_{92}Al_8$	2w 1000 (g)	fcc (A_1)	3.542	27	−0.11	−0.13	4.1
$Ni_{92}Si_8$	2w 1000 (g)	fcc (A_1)	3.519	17	−0.09	−0.09	5.3
$Ni_{92}Ga_8$	2w 1000 (g)	fcc (A_1)	3.545	29	−0.14	−0.17	4.8
$Ni_{92}Ge_8$	as-cast	fcc (A_1)	3.542	23	−0.07	−0.08	3.0
$Ni_{92}V_8$	as-cast	fcc (A_1)	3.539	1.2	0.00	0.00	–
$Ni_{92}Pd_8$	as-cast	fcc (A_1)	3.562	51	−0.21	−0.22	4.1
$Ni_{92}Pt_8$	as-cast	fcc (A_1)	3.564	43	−0.32	−0.30	7.4
$Ni_{92}Nb_8$	as-cast	fcc (A_1)	3.564	4.8	0.00	−0.01	–
$Ni_{92}Ta_8$	as-cast	fcc (A_1)	3.584	1.0	0.00	0.00	–
$Ni_{92}Au_8$	3d 900 (q)	fcc (A_1)	3.584	38	−0.19	−0.20	5.0
$Ni_{92}Sn_8$	3d 900 (q)	fcc (A_1)	3.601	30	−0.06	−0.07	2.0
$Ni_{92}In_8$	3d 900 (q)	fcc (A_1)	3.598	24	−0.07	−0.08	2.9
$Ni_{92}Ti_8$	as-cast	fcc (A_1)	3.556	10	−0.01	−0.03	1.0
$Ni_{92}W_8$	as-cast	fcc (A_1)	3.562	0.6	0.00	0.00	–
$Ni_{92}Cr_8$	as-cast	fcc (A_1)	3.530	2.6	−0.02	−0.01	–

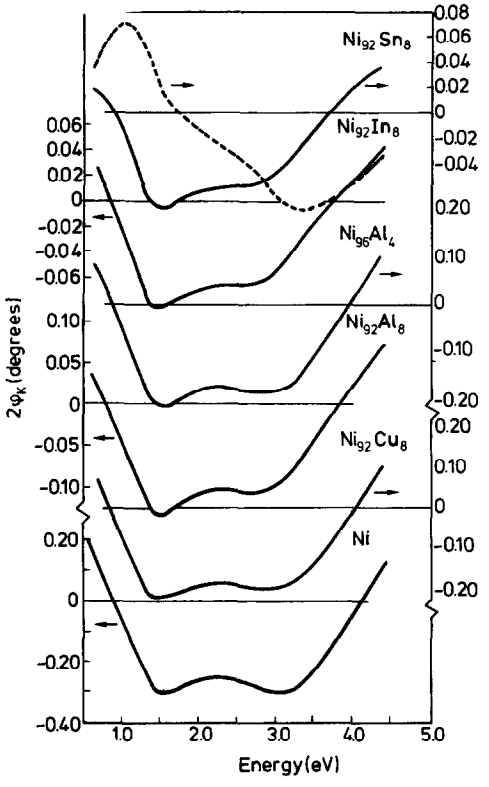

Fig. 1. Energy dependence of the Kerr rotation ($2\varphi_K$) in various Ni-base alloys. For the alloy $Ni_{92}Sn_8$ the ellipticity ($2\epsilon_K$) is also shown (broken line).

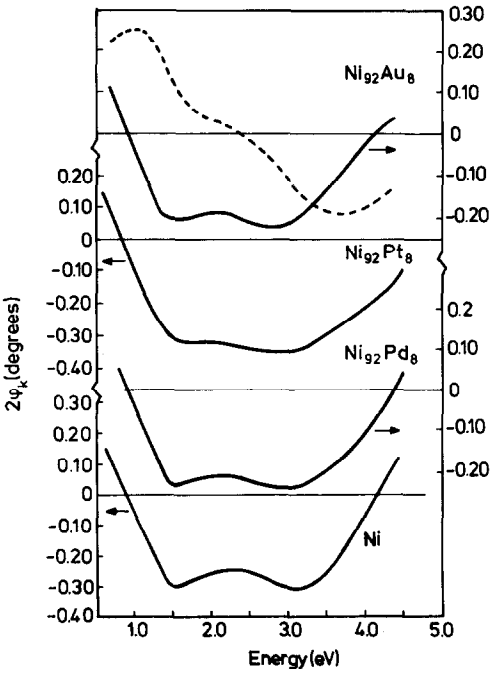

Fig. 2. Energy dependence of the Kerr rotation ($2\varphi_K$) in various Ni-base alloys. For the alloy $Ni_{92}Au_8$ the ellipticity ($2\epsilon_K$) is also shown (broken line).

applies to the energy where the second sign reversal of φ_k occurs (at about 4 eV). No substantial changes occur upon alloying with Cu. In fig. 2 we show some results obtained on alloys where Ni is combined with noble metals. The spectrum of the Au alloy resembles that of the Cu alloy shown in fig. 1. In both cases there is only a modest decrease in amplitude and almost no shifts of the energies corresponding to the sign reversal. The alloys with Pt and Pd show quite an interesting behaviour. In contrast to the spectra of the alloys with Al, In and Sn their spectra give rise to a high-energy sign reversal of $\varphi_K(E)$ which is shifted to higher rather than lower energies. This feature is particularly pronounced in the case of Pt.

For the remainder of Ni alloys investigated we present only the values of $2\varphi_K$ at the two different wavelengths mentioned in section 2.2. These values, together with the room temperature magnetization and some crystallographic data, are collected in table 1.

3.2. Co-base materials

The results obtained for Ga–Co alloys can be regarded as examples of the changes in magneto-optical properties of Co when this latter element is combined with an s, p metal. The various spectra measured in this system are shown in fig. 3. Alloying is seen to lead to a reduction in amplitude. Apart from this effect one may notice that increasing Ga concentration leads to a shift of the low-energy peak to higher energies while the high-energy peak shifts in the opposite direction, resulting eventually in a coalescence of both peaks. A somewhat different behaviour is observed when Co is combined with early transition metals such as Ti, Zr, Hf or Nb. Results for several Hf–Co compounds are shown in fig. 4. It is seen that the low-energy peak does not shift. Only the high

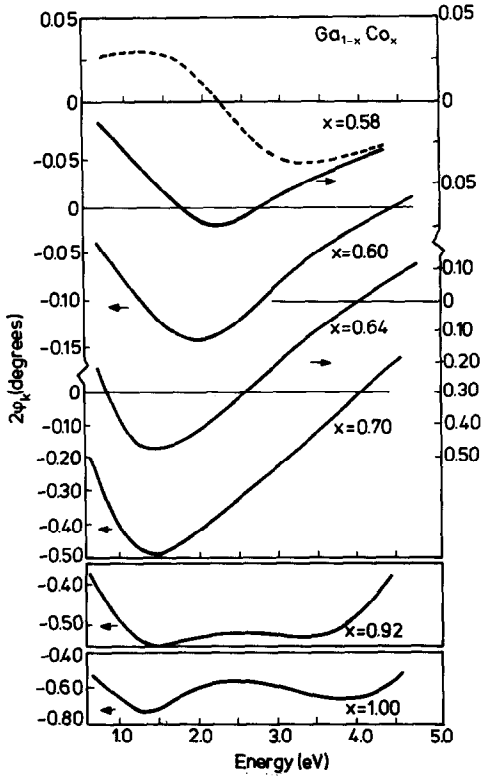

Fig. 3. Energy dependence of the Kerr rotation ($2\varphi_K$) in several $Ga_{1-x}Co_x$ alloys and compounds. For $x = 0.58$ the ellipticity ($2\epsilon_K$) is also shown (broken line).

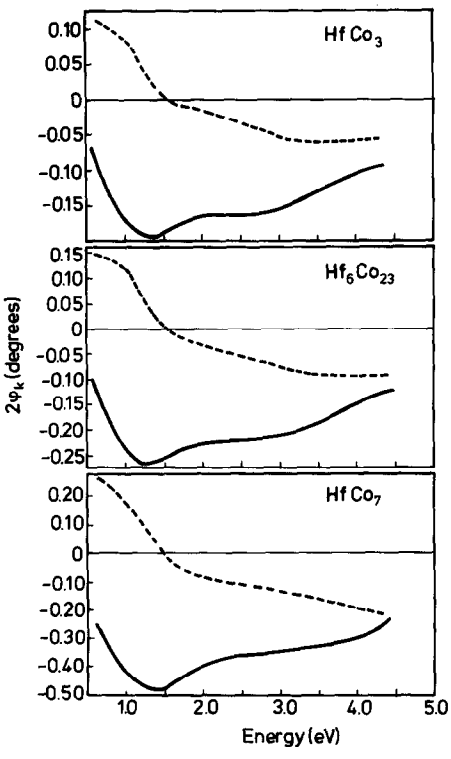

Fig. 4. Energy dependence of the Kerr rotation ($2\varphi_K$) in several Hf–Co compounds. The ellipticity ($2\epsilon_K$) is also shown (broken line).

energy peak shifts to lower energies. In these cases, too, alloying leads to a reduction in the Kerr amplitude, to a larger extent for the high-energy peak than for the low-energy peak. The behaviour is different when Co is alloyed with a non-magnetic late transition metal. Results for Pd–Co alloys are shown in fig. 5. There is almost no reduction in Kerr amplitude while the second peak has now increased in intensity relative to the first peak. Results for Pt–Co alloys are shown in fig. 6. In these alloys too the relative contribution of the second peak increases, as it does in the Pd–Co system. Comparison of the results shown in fig. 5 with the structural data listed in table 2 for Pt–Co makes it clear that structural changes have little effect on the Kerr spectra. The same findings were obtained from a detailed study of $Co_{75}Pt_{25}$. As-cast alloys did not give rise to spectra different from those of alloys annealed at low temperatures (100–500°C). Table 2 contains also the results obtained on various other Co-base materials not yet mentioned in this section.

3.3. Fe-base materials

Typical examples of Kerr spectra pertaining to compounds in which Fe is combined with an s, p element are shown in fig. 7. The changes are seen to affect primarily the high-energy side of the spectra while the location of the low-energy maximum of φ_K is more or less preserved in the Fe-rich concentration range. A similar behaviour was also observed in the series Fe–Al and Fe–Ga. Results for alloys in which Fe is combined with Pd or Pt

Table 2
Crystalchemical, magnetic and magneto-optic data of Co alloys and Co compounds. The σ- and $2\varphi_K$ values represent the room temperature magnetization and the room temperature polar Kerr rotation angle, respectively

Alloy or compound	Heat treatment	Crystal structure	Lattice constants (Å)	σ (Am^2kg^{-1})	$2\varphi_K$ (deg)		$\frac{2\lvert\varphi_K\rvert}{\sigma} \times 10^3$
					633 nm	830 nm	
Co	as-cast	hcp (A_3)	$a = 2.497$; $c = 4.059$	156	−0.70	−0.78	4.5
Co_3B	3 w 1000	0.rh (DO_{11})	$a = 4.432$; $b = 5.229$; $c = 6.631$	82	−0.51	−0.49	6.2
Co_2B	as-cast	tetr (C16)	$a = 5.014$; $c = 4.215$	47	−0.15	−0.10	3.2
Co_2Mg	14 d 900	hex (C14)	$a = 4.859$; $c = 8.954$	55	−0.66	−0.69	12
CoZn	7 d 900 (q)	cub (A_{13})	$a = 6.319$	39	−0.25	−0.25	6.4
$Co_{92}Ga_8$	14 d 1000 (q)	hcp (A_3)	$a = 2.522$; $c = 4.096$	133	−0.71	−0.74	5.3
$Co_{70}Ga_{30}$	5d 1100 (q)	cub (B2)	$a = 2.862$	62	−0.41	−0.48	6.6
$Co_{68}Ga_{32}$	5d 1100 (q)	cub (B2)	$a = 2.872$	52	−0.34	−0.35	6.5
$Co_{64}Ga_{36}$	5d 1100 (q)	cub (B2)	$a = 2.862$	32	−0.41	−0.47	12.8
$Co_{60}Ga_{40}$	5d 1100 (q)	cub (B2)	$a = 2.875$	4.9	−0.14	−0.12	28.6
$Co_{58}Ga_{42}$	5d 1100 (q)	cub (B2)	$a = 2.876$	1.3	−0.07	−0.05	54
$Co_{90}Si_{10}$	as-cast	hcp (A_3)	$a = 2.507$; $c = 4.065$	126	−0.62	−0.68	4.9
Co_3Si	7h 1180 (q)	–	–	47	−0.26	−0.28	5.5
Co_2Si	3d 1100	0.rh. (C37)	$a = 4.891$; $b = 3.725$; $c = 7.087$	0.16	−0.04	−0.03	–
Co_7Ge_3	30d 900			23	−0.14	−0.15	6.1
$Co_{90}Sn_{10}$	as-cast	cph (A_3)	$a = 2.522$; $c = 4.159$	115	−0.58	−0.65	5.0
Co_2Sn	3 d 1050 (q)	hex ($B8_2$)	$a = 4.116$; $c = 5.023$	17	−0.10	−0.11	5.9
$CoSn_2$	40 d 460	tetr (C16)	$a = 6.375$; $c = 5.446$	≈ 0	0.00	0.00	–
Co_2P	–	0.rh. (C23)	$a = 5.83$; $b = 3.70$; $c = 6.75$	20	−0.04	−0.12	2.0
$Co_{80}Ti_{20}$	20d 800	fcc ($L1_2$)	$a = 3.606$	25	−0.29	−0.31	11.6
$Co_{77}Ti_{23}$	14d 900	fcc ($L1_2$)	$a = 3.615$	8	−0.17	−0.17	21.3
$Co_{75}Ti_{25}$	20d 900	fcc ($L1_2$)	$a = 3.628$	1	−0.11	−0.10	110
$Co_{11}Zr_2$	–	–	–	72	−0.30	−0.34	4.2
$Co_{23}Zr_6$	10d 900	cub ($D8_a$)	$a = 11.561$	49	−0.18	0.20	3.7

Co_7Hf	30d 1150 (q)	tetr.	$a = 7.070$; $c = 7.999$	74	−0.40	−0.47	5.4
$Co_{23}Hf_6$	30d 1000 (q)	cub ($D8_a$)	$a = 11.502$		−0.23	−0.26	
$Co_{3.2}Hf$	5d 1100 (q)	fcc (C15)	$a = 6.815$	19	−0.17	−0.19	8.9
$Co_{75}Ta_{25}$	3 w 900	fcc (C15)	$a = 6.788$	0.2	0.00	0.00	–
$Co_{94}Cr_6$	as-cast	hcp (A_3)	$a = 2.505$; $c = 4.059$	125	−0.53	−0.63	4.2
$Co_{88}Cr_{12}$	14d 700	hcp (A_3)	$a = 2.513$; $c = 4.059$	78	−0.38	−0.46	4.1
$Co_{80}Cr_{20}$	as-cast	hcp (A_3)	$a = 2.520$; $c = 4.062$	40	−0.21	−0.25	5.3
$Co_{75}Cr_{25}$	as-cast	hcp (A_3)	$a = 2.525$; $c = 4.065$	6.5	−0.09	−0.11	13.8
Co_2Cr_3	10d 100	tetr ($D8_b$)	$a = 8.785$; $c = 4.553$	0.1	−0.01	−0.00	–
$Co_{90}Mo_{10}$	as-cast	hcp (A_3)	$a = 2.540$; $c = 4.105$	94	−0.38	−0.46	4.0
Co_9Mo_2	14d 1000 (q)	hex (DO_{19})	$a = 5.194$; $c = 4.212$	35	−0.18	−0.22	5.1
$Co_{80}Mo_{20}$	as-cast	hcp (A_3)	$a = 2.562$; $c = 4.177$	29	−0.14	−0.17	4.8
Co_3Mo	20d 900	hex (DO_{19})	$a = 5.142$; $c = 4.133$	0.6	−0.01	−0.01	–
$Co_{90}W_{10}$	as-cast	hcp (A_3)	$a = 2.535$; $c = 4.111$	82	−0.36	−0.46	4.4
$Co_{85}W_{15}$	as-cast	hcp (A_3)	$a = 2.544$; $c = 4.146$	45	−0.27	−0.34	6.0
$Co_{80}W_{20}$	as-cast	fcc (A_1)	$a = 3.268$	19	−0.17	−0.21	8.9
$Co_{85}Pd_{15}$	as-cast	fcc (A_1)	$a = 3.621$	133	−0.68	−0.76	5.1
$Co_{65}Pd_{35}$	as-cast	fcc (A_1)	$a = 3.705$	101	−0.50	−0.51	5.0
CoPd				78	−0.38	−0.35	4.9
$Co_{85}Rh_{15}$	as-cast	hcp (A_3)	$a = 2.553$; $c = 4.129$	134	−0.60	−0.66	4.5
$Co_{75}Rh_{25}$	as-cast	hcp (A_3)	$a = 2.581$; $c = 4.158$	112	−0.51	−0.54	4.5
$Co_{65}Rh_{35}$	as-cast	hcp (A_3)	$a = 2.602$; $c = 4.190$	88	−0.41	−0.43	4.7
$Co_{85}Ir_{15}$	as-cast	hcp (A_3)	$a = 2.556$; $c = 4.123$	88	−0.48	−0.53	5.5
$Co_{75}Ir_{25}$	as-cast	hcp (A_3)	$a = 2.581$; $c = 4.158$	53	−0.36	−0.41	6.8
$Co_{65}Ir_{35}$	as-cast	hcp (A_3)	$a = 2.602$; $c = 4.183$	30	−0.27	−0.30	9.0
$Co_{90}Pt_{10}$	as-cast	hcp (A_3)	$a = 2.550$; $c = 4.122$	123	−0.75	−0.79	6.1
$Co_{80}Pt_{20}$	as-cast	hcp (A_3)	$a = 2.570$; $c = 4.189$	91	−0.59	−0.60	6.5
$Co_{75}Pt_{25}$	as-cast	fcc (A_1)	$a = 3.668$	83	−0.72	−0.75	8.7
$Co_{70}Pt_{30}$	as-cast	fcc (A_1)	$a = 3.694$	76	−0.80	−0.87	10.5
$Co_{58}Pt_{42}$	5 d 320	fcc (A_1)	$a = 3.744$	56	−0.75	−0.83	13.4
	as-cast	fcc (A_1)	$a = 3.745$		−0.68	−0.74	–
$Co_{50}Pt_{50}$	7 d 600	fct ($L2_0$)	$a = 3.795$; $c = 3.689$	30	−0.67	−0.73	22.3
	as-cast	fcc (A_1)	$a = 3.776$		−0.59	−0.64	–
$Co_{30}Pt_{70}$	5 d 320	fcc (A_1)	$a = 3.842$	29	−0.50	−0.51	17.2
	as-cast	fcc (A_1)	$a = 3.842$		−0.47	−0.48	–

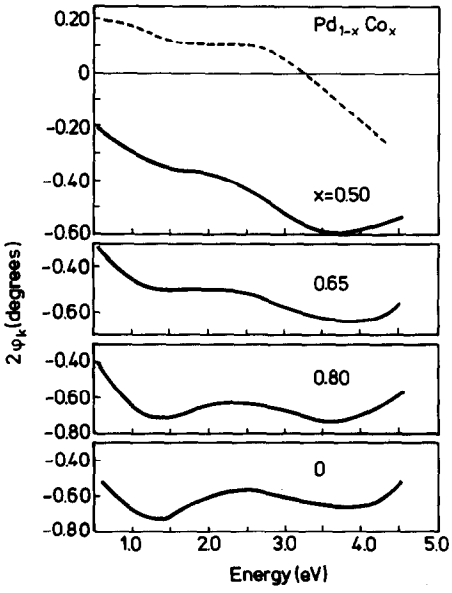

Fig. 5. Energy dependence of the Kerr rotation ($2\varphi_K$) in several $Pd_{1-x}Co_x$ alloys and compounds. For PdCo the ellipticity ($2\epsilon_K$) is also shown (broken line).

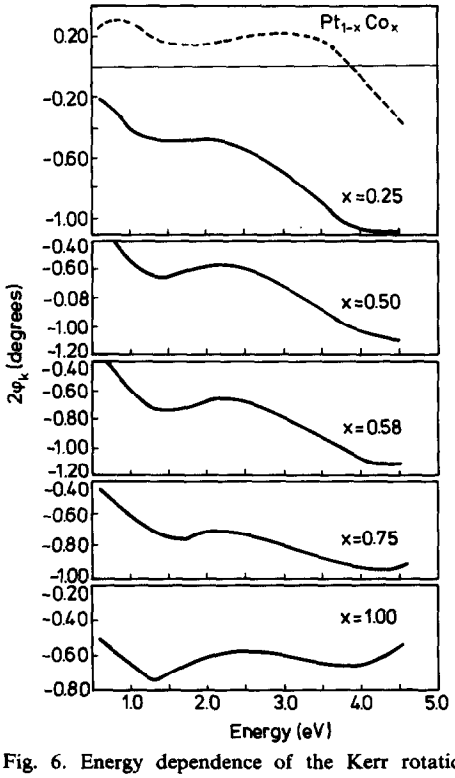

Fig. 6. Energy dependence of the Kerr rotation ($2\varphi_K$) in several $Pd_{1-x}Co_x$ alloys and compounds. For $x = 0.25$ the ellipticity ($2\epsilon_K$) is also shown (broken line).

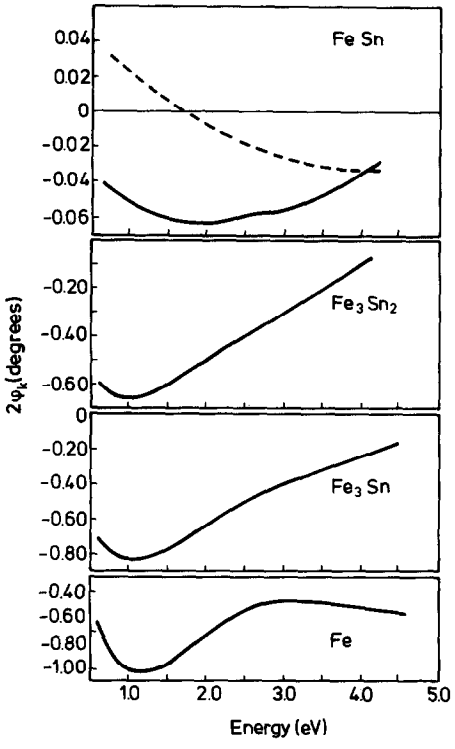

Fig. 7. Energy dependence of the Kerr rotation ($2\varphi_K$) in several Fe–Sn compounds. For FeSn the ellipticity ($2\epsilon_K$) is also plotted (broken line).

are shown in fig. 8. Here one notices again that there is a substantial increase in the relative intensity of the second peak. Data for other Fe-base systems have been collected in table 3.

3.4. Mn-base materials

Compared to the Fe- and Co-base materials alloying of Mn with other metals does not lead to many ferromagnetic alloys or compounds. The reason is different from the on that applies in the Ni systems. With Mn alloys or compounds it is not the size of the moment that becomes strongly reduced upon alloying but rather the tendency of the Mn moments to couple antiferromagnetically. Results obtained on Mn compounds having a sufficiently strong magnetization at room temperature are listed in table 4. The Kerr spectrum obtained for $Mn_{56}Ga_{44}$ is shown in fig. 9. Spectra

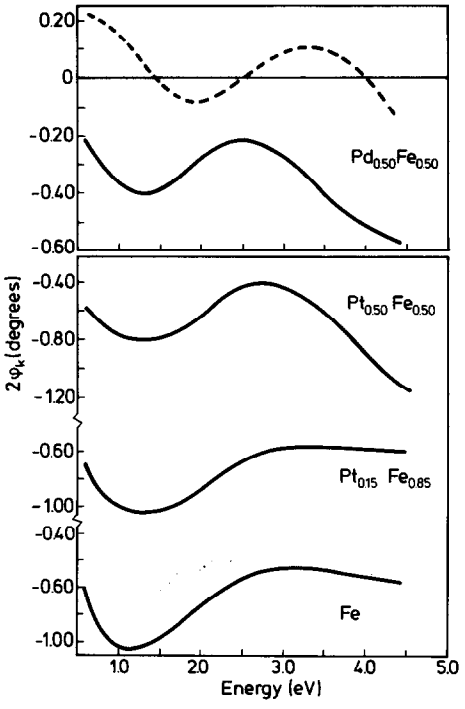

Fig. 8. Energy dependence of the Kerr rotation ($2\varphi_K$) in PdFe and PtFe. For PdFe the ellipticity is also plotted (broken line).

of two Mn–Sb compounds are shown in fig. 10. Since Mn is not magnetic, a comparison with the unalloyed parent material cannot be made. The examples shown in figs. 9 and 10 serve to illustrate that with Mn-base materials a large variety of different types of spectra is observed, comprising energy dependencies of φ_K which increase with E (Fig. 9) from negative φ_K to positive φ_K, decrease

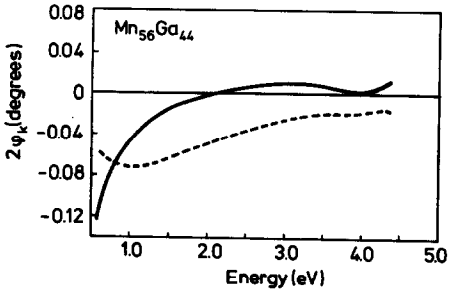

Fig. 9. Kerr spectrum of $Mn_{56}Ga_{46}$. Full line: Kerr rotation ($2\varphi_K$); broken line: ellipticity.

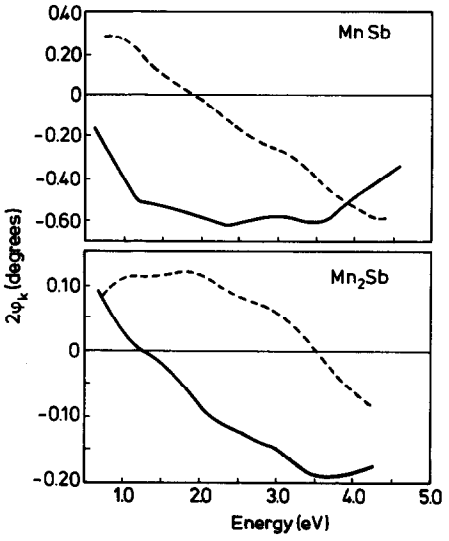

Fig. 10. Kerr spectra of the compounds MnSb and Mn_2Sb. Full line: Kerr rotation ($2\varphi_K$); broken line: ellipticity.

with E from positive φ_K to negative φ_K (fig. 10 bottom part), or do not give rise to a sign reversal with increasing E (upper part of fig. 10). Data for other Mn-base materials are given in table 4.

3.5. *Ternary and pseudo-binary compounds*

There exists a rather large group of intermetallic compounds in which a given 3d metal is compounded with two other metals. These comprise pseudo-binary compounds like $Zr(Fe_{1-x}Al_x)_2$ or $Gd(Fe_{1-x}Al_x)_2$ where one of the components is replaced by another without giving rise to an a new type of crystal structure. This group also comprises true ternaries like those in the low-temperature phase of MnAlGe where the atoms of the components reside on non-equivalent crystallographic sites [11]. Results for the low-temperature MnAlGe phase are shown in fig. 11. A large variety of different pseudo-binary and ternary compounds can be seen in table 5. Note that the magnetization of the compounds $Al_5Mn_3T_2$ (T = Fe, Co, Ni, Cu) has substantial room temperature values even though the Kerr amplitude observed in these compounds is extremely small at the two wavelengths considered. (In fact the Kerr effect

Table 3
Crystalchemical, magnetic and magneto-optic data of Fe compounds and alloys. The magnetization (σ) and polar Kerr rotation angle ($2\varphi_K$) were measured at room temperature in an applied field of 1280 kA/m

Alloy or compound	Heat treatment	Crystal structure	Lattice constants (Å)	σ (Am^2kg^{-1})	$2\varphi_K$(deg)		$\frac{2\lvert\varphi_K\rvert}{\sigma} \times 10^3$
					633 nm	830 nm	
Fe	as-cast	bcc (A_2)	$a = 2.867$	213	−0.82	−1.07	3.85
$Fe_{90}Al_{10}$	10 d 1000 (q)	bcc (A_2)	$a = 2.886$	203	−0.83	−1.07	3.1
$Fe_{80}Al_{20}$	10 d 1000 (q)	bcc (A_2)	$a = 2.907$	185	−0.78	−0.94	4.2
$Fe_{75}Al_{25}$	10 d 1000 (q)	bcc (A_2)	$a = 2.911$	162	−0.79	−0.95	4.9
Fe_3Al	30 d 440	fcc (DO_3)	$a = 5.805$	156	−0.79	−0.96	5.1
$Fe_{70}Al_{30}$	30 d 600	bcc (A_2)	$a = 2.919$	98	−0.69	−0.82	7.8
$Fe_{80}Ga_{20}$	20 d 600	bcc (A_2)	$a = 2.907$	167	−0.90	−1.12	5.4
Fe_7Ga_3	30 d 600	fcc ($L1_2$)	$a = 3.683$	147	−0.91	−1.13	6.2
$Fe_{70}Ga_{30}$	10 d 900 (q)	bcc (A_2)	$a = 2.930$	107	−0.85	−1.04	7.9
Fe_2Ga	6 d 650 (q)	bcc (A_2)	$a = 2.917$	92	−0.78	−0.90	8.5
Fe_3Ga_2	18 d 900 (q)	bcc (A_2)	$a = 2.89$	101	−0.69	−0.88	6.8
Fe_3Ga_4	90 d 800	monocl.	–	24	−0.33	−0.38	13.8
Fe_3C	as-cast	0.rh (DO_{11})	$a = 5.055$; $b = 4.4.513$; $c = 6.681$	100	−0.42	−0.49	4.2
$Fe_{80}Si_{20}$	20 d 900	bcc (A_1)	$a = 2.848$	160	−0.73	−0.85	4.6
Fe_3Si	20 d 900	fcc ($L2_1$)	$a = 5.662$	138	−0.65	−0.72	4.7
Fe_5Si_3	20 d 900	hex ($D8_8$)	$a = 6.755$; $c = 4.714$	76	−0.34	−0.50	4.5
Fe_2B	as-cast	tetr. (C16)	$a = 5.110$; $c = 4.183$	166	−0.90	−0.94	5.4
FeB	as-cast	0.rh. (B27)	$a = 5.502$; $b = 2.951$; $c = 4.062$	84	−0.53	−0.45	6.3
$Fe_{90}Ge_{10}$	20 d 900	bcc (A_1)	$a = 2.893$	191	−0.87	−1.10	4.6
$Fe_{85}Ge_{15}$	20 d 900	bcc (A_1)	$a = 2.900$	169	−0.88	−1.11	5.2
Fe_3Ge	10 d 1000	hex (DO_{19})	$a = 5.179$; $c = 4.227$	133	−0.82	−0.89	6.2
$Fe_{62}Ge_{38}$	as-cast	hex ($B8_2$)	$a = 4.011$; $c = 5.023$	69	−0.54	−0.51	7.8
$Fe_{59}Ge_{41}$	10 d 900 (9)	hex ($B8_2$)	$a = 3.974$; $c = 4.992$	35	−0.35	−0.32	10.0
Fe_3Sn	20 d 800 (q)	hex (DO_{19})	$a = 5.457$; $c = 4.362$	126	−0.63	−0.76	5.0
Fe_3Sn_2	35 d 700 (q)	monocl.	–	69	−0.49	−0.59	7.1
FeSn	30 d 600	hex (B35)	$a = 5.307$; $c = 4.445$	0.6	−0.06	−0.06	

Fe_2Sc	3 d 1100 (q)	hex (C14)	$a = 4.957$; $c = 8.110$	52	−0.34	−0.34	6.5
$Fe_{74}Ti_{26}$	6h 1180 (q)	hex (C14)	$a = 4.780$; $c = 7.771$	74	−0.20	−0.24	2.7
$Fe_{72}Ti_{28}$	3 w 900	hex (C14)	$a = 4.800$; $c = 7.824$	36	−0.09	−0.12	2.5
$Fe_{69}Zr_{31}$	12 d 1000 (q)	cub (C15)	$a = 7.064$	91	−0.48	−0.53	5.3
$Fe_{74}Zr_{26}$	12 d 1000 (q)	cub (C15)	$a = 7.019$	74	−0.40	−0.52	5.4
Fe_2Hf	as-cast	hex (C14)	$a = 4.968$; $c = 8.098$	45	−0.64	−0.71	14.2
$Fe_{74}Hf_{26}$	8h 1200 (q)	hex (C14)	$a = 4.985$; $c = 8.074$	57	−0.50	−0.67	8.8
$Fe_{80}V_{20}$	as-cast	bcc (A_2)	$a = 2.892$	156	−0.55	−0.73	3.5
FeV	1 m 900	tetr. ($D8_b$)	$a = 8.917$; $c = 4.610$	0.3	0.00	0.00	0.0
$Fe_{77}Nb_{23}$	14 d 1000 (q)	hex (C14)	$a = 4.809$; $c = 7.837$	36	−0.08	−0.12	2.2
$Fe_{70}Nb_{30}$	14 d 1000 (q)	hex (C14)	$a = 4.845$; $c = 7.893$	0.9	0.00	0.00	0.0
FeCr	3 w 600 (q)	tetr ($D8_b$)	$a = 8.802$; $c = 4.548$	2.4	−0.15	−0.16	63.0
$Fe_{68}W_{32}$	3 w 900	hex (C14)	$a = 4.756$; $c = 7.735$	27	−0.12	−0.21	4.4
Fe_3Co	90 d 500	bcc (A_2)	$a = 2.867$	234	−0.83 *	−0.93 *	3.5
FeCo	30 d 600	bcc (A_2)		230	−1.08 *	−1.21 *	4.7
$FeCo_3$	20 d 460	bcc (A_2)	$a = 2.842$	200	−0.96 *	−1.16 *	4.8
$FeNi_3$	30 d 440	fcc (A_1)	$a = 3.564$	108	−0.46	−0.35	4.3
$Fe_{85}Pd_{15}$				190	−0.76	−0.90	4.0
$Fe_{75}Pd_{25}$	100 d 350	fcc ($L1_2$)	$a = 3.818$	58	−0.06	−0.05	1.0
	as-cast	bcc (A_2)	$a = 2.962$	167	−0.66	−0.75	4.0
$Fe_{65}Pd_{35}$	as-cast	fcc (A_1)	$a = 3.785$	138	−0.50	−0.57	3.6
$Fe_{50}Pd_{50}$	120 d 600	fcc ($L1_2$)	$a = 3.837$	96	−0.29	−0.39	3.0
$Fe_{45}Pd_{55}$	4 w 600	fct ($L2_0$)		88	−0.22	−0.32	2.5
$Fe_{85}Pt_{15}$	as-cast	bcc (A_2)	$a = 2.936$	172	−1.05	−1.23	6.1
Fe_3Pt	6 w 670 (q)	fcc ($L1_2$)	$a = 3.730$	107	−1.03	−1.16	9.6
$Fe_{65}Pt_{35}$	as-cast	fcc (A_1)	$a = 3.779$	92	−0.88	−0.96	9.6
$Fe_{55}Pt_{45}$	as-cast	fct ($L2_0$)	$a = 3.840$; $c = 3.727$	45	−0.73	−0.88	16.2
FePt	3 w 900	fct ($L2_0$)	$a = 3.905$; $c = 3.735$	42	−0.64	−0.79	15.2

* Values may be 10% too low to imperfect magnetical saturation.

Table 4
Crystalchemical magnetic and magneto-optic data of several Mn compounds. The magnetization (σ) and the polar Kerr rotation angle were measured at room temperature in a field of 1280 kA/m

Alloy or compound	Heat treatment	Crystal structure	Lattice constants (Å)	σ ($Am^2\,kg^{-1}$)	$2\varphi_K$ (deg)		$\frac{2\lvert\varphi_K\rvert}{\sigma} \times 10^3$
					633 nm	830 nm	
$Mn_{56}Ga_{44}$	600 (q)	cub	$a = 3.593$	60	0.00	−0.01	0.0
Mn_2Ga	3 w 560	fct ($L1_0$)	$a = 2.754$; $c = 3.590$	> 36	+0.02	+0.02	0.6
$Mn_{72}Ga_{28}$	75 h 700 (q)	hcp (A_3)	$a = 2.707$; $c = 4.333$	5.4	0.00	0.00	–
$Mn_{23}Y_6$	15 d 850	cub (D8a)	$a = 12.445$	33	0.00	0.00	0.0
$Mn_{23}Gd_6$	15 d 850	„ (D8a)	$a = 12.515$	45	0.00	0.00	0.0
Mn_3In	20 d 500	cub ($D8_2$)	$a = 9.400$	0.7	0.00	0.00	–
$MnNi_3$	3 w 375	cub ($L1_2$)	$a = 3.593$	27	0.00	0.0	
MnV	3 w 600	fcc	$a = 5.808$	0.1	0.00	+0.01	–
Mn_2Sn	3 w 600	hex (B8)	$a = 4.404$; $c = 5.529$	4.0	0.00	0.00	
$Mn_{45}Ni_{55}$	6 w 600	tetr $L1_0$	–	0.3	+0.01	+0.01	–
MnNi	7 w 800 (q)	tetr $L1_0$	$a = 3.723$; $c = 3.520$	0.3	+0.01	+0.01	–
MnPt							
$MnPt_2$	as-cast	cub	$a = 3.900$	1.9			
$MnPt_3$	as-cast	cub ($L1_2$)	$a = 3.900$	14.9	0.00	0.00	0.0
Mn_5Ge_2	4 w 460	–	–	5	−0.01	+0.01	–
MnSb	1 w 600	hex (B8)	$a = 4.120$; $c = 5.790$	99	−0.58	−0.54	5.9
Mn_2Sb	1 w 600	tetr (C38)	$a = 4.062$; $c = 6.534$	29	−0.08	−0.02	2.8

appeared to be very low in the whole spectral region considered here.)

A special group of ternary consists of the so-called Heusler alloys. Experimental data of the cubic $L2_1$ type compounds have been collected in tables 6–9. The Kerr spectra of these compounds show a wide variety in shape and Kerr amplitude [12]. In the case of Co_2YSn (Y = Ti, Zr, Hf) we were able to interpret the energy dependence of φ_K in terms of charge transfer spectra [13]. For the majority of the many spectra recorded we are not yet able to give a meaningful interpretation. Three spectra of Heusler alloys of the type Cu_2MnZ

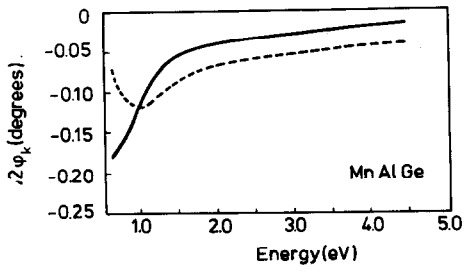

Fig. 11. Kerr spectra of MnAlGe after vacuum annealing.

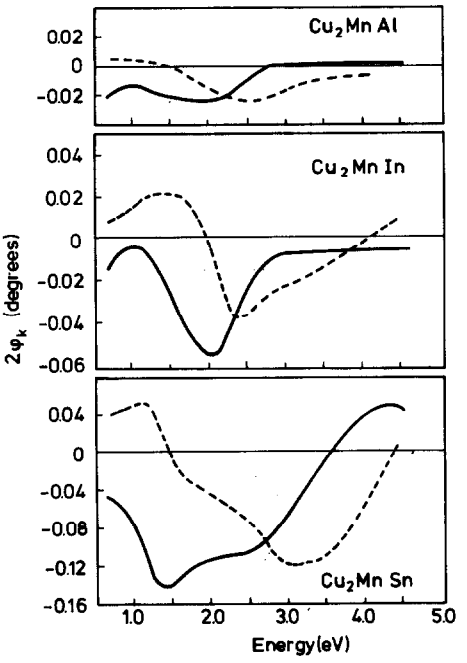

Fig. 12. Kerr spectra of several Heusler compounds of the type Cu_2MnX. Full line: Kerr rotation ($2\varphi_K$); broken line: ellipticity.

Table 5
Crystal-chemical, magnetic and magneto-optic data of some ternary and pseudo-binary 3d transition metal compounds. The magnetization (σ) and the polar Kerr rotation angle ($2\varphi_K$) were obtained at room temperature in a field of 1280 kA/m

Compound	Heat treatment	Crystal structure	Lattice constants (Å)	σ (Am^2kg^{-1})	$2\varphi_K$ (deg)		$\frac{2\lvert\varphi_K\rvert}{\sigma} \times 10^3$
					633 nm	830 nm	
$ZrFe_{3.3}Al_{1.3}$	20 d 800	hex (C14)	$a = 4.987$; $c = 8.095$	35	−0.17	−0.23	4.9
GdFeAl	3 d 1100 (q)	hex (C14)	$a = 5.445$; $c = 8.809$	–	0.00	+0.02	–
$GdFe_{1.2}Al_{0.8}$	3 d 1100 (q)	hex (C44)	$a = 5.388$; $c = 8.709$	–	+0.09	+0.13	–
$Zr_{0.8}Mo_{0.2}Fe_2$	as-cast	fcc (C15)	$a = 7.05$	19	−0.03	−0.02	1.6
$Zr_{0.75}Nb_{0.25}Fe_2$	as-cast	fcc (C15)	$a = 7.038$	58	−0.30	−0.32	5.2
$ZrFe_{1.76}V_{0.24}$	as-cast	fcc (C15)	$a = 7.069$	40	−0.11	−0.18	2.8
$Zr_6Co_{16}Ge_7$	3d 1100 (q)	cub ($D8_a$)	$a = 11.62$	1	0.00	0.00	–
$LaCo_{11}Si_2$	20 d 800	cub ($D2_3$)	$a = 11.28$	77	−0.36	−0.42	4.7
$Fe_{2.4}V_{0.6}Ge$	14 d 800 (q)	bcc (A_2)	$a = 2.882$	43	−0.42	−0.41	9.8
$Fe_{2.7}V_{0.3}Ge$	14 d 800 (q)	hex	$a = 4.250$; $c = 5.741$	97	−0.72	−0.70	7.4
Mn_2MoB_4	as-cast	0.rh ($D7_b$)	$a = 3.17$; $b = 13.02$; $c = 3.01$	32	−0.10	−0.08	3.1
Mn_2CrB_4	as-cast	unknown	–	10	0.00	0.00	0.0
MnAlGe	30 d 500	tetr. (C38)	$a = 3.890$; $c = 5.925$	40	−0.04	−0.05	1.0
$Al_5Mn_3Ni_2$	25 d 900	cub (B2)	$a = 2.940$	45.2	−0.01	−0.02	0.2
$Al_5Mn_3Co_2$	25 d 900	cub (B2)	$a = 2.937$	43.8	−0.02	−0.04	0.5
$Al_5Mn_3Cu_2$	as-cast	cub (B2)	$a = 2.979$	70.2	0.00	0.00	0.0
$Al_5Mn_3Fe_2$	25 d 900	cub (B2)	$a = 2.955$	–	−0.02	−0.02	–

Table 6
Lattice constant (a), Curie temperature (T_c), saturation moment at 4.2 K (μ_s) saturation magnetization at 300 K (σ) and Kerr rotation ($2\varphi_K$) measured in various Heusler alloys. The values of T_c of Co_2MnAl, Co_2VAl and Co_2HfAl were taken from literature: (a) ref. [14]; (b) ref. [15]

Compound	Heat treatment	a (Å)	T_C (K)	μ_s (μ_B/FU)	σ ($Am^2 kg^{-1}$)	$2\varphi_K$ (deg)		$\frac{2\lvert\varphi_K\rvert}{\sigma} \times 10^3$
						633 nm	830 nm	
Mn_2VAl	30 d 800	5.897	–	1.82	50	+0.02	+0.01	0.4
Fe_2NiAl	30 d 600	5.758	–	4.25	117	−0.50	−0.61	4.3
Fe_2MnAl	12 d 900	5.816	–	1.58	52	−0.25	−0.28	4.8
Fe_2CrAl	11 d 800	5.805	246	1.67	–	−0.22	−0.24	–
Fe_2VAl	11 d 800	5.761	–	$\chi_g = 1.8\times10^{-5}$ emu/g		–	–	–
Fe_2TiAl	14 d 900	5.879	123	0.11	–	–	–	–
Fe_2MoAl	as cast	5.918	–	0.36	–	–	–	–
Co_2FeAl	10 d 800	5.730	–	4.96	138	−0.74	−0.84	5.4
Co_2MnAl	as-cast	5.749	693 (a)	4.04	104	−0.09	−0.08	0.9
Co_2CrAl	as-cast	5.727	334	1.55	17	−0.02	−0.02	1.2
Co_2VAl	as-cast	5.772	310 (b)	1.95	27	−0.03	−0.03	1.1
Co_2TiAl	14 d 800	5.847	134	0.74	–	–	–	–
Co_2NbAl	10 d 900	5.935	383	1.35	22	−0.01	−0.01	0.5
Co_2ZrAl	3 d 1050	6.078	178	0.79	–	–	–	–
Co_2TaAl	10 d 900	5.930	260	1.50	–	–	–	–
Co_2HfAl	3 d 1000	6.045	193 (b)	0.82	–	–	–	–
Ni_2MnAl	8d 900	5.824	$T_N = 30$	–	–	–	–	–
Ni_2CrAl	sp.c	5.737	140	0.13	–	−0.02	−0.02	–
Cu_2MnAl	10 d 800	5.968	603	3.60	86	–	–	–

Table 7
Lattice constants (a), Curie temperatures (T_c), saturation moments at 4.2 K (μ_s), saturation magnetization at 300 K (σ) and Kerr rotation ($2\varphi_K$) observed in various Heusler alloys of the type X_2YGa. For T_C some literature values are included: (a) ref. [14]; (b) ref. [15]; (c) ref. [16]

Compound	Heat treatment	a (Å)	T_c (K)	μ_s (μ_B/F.U.)	σ ($Am^2 kg^{-1}$)	$2\varphi_K$ (deg)		$\frac{2\lvert\varphi_K\rvert}{\sigma} \times 10^3$
						633 nm	830 nm	
Mn_2VGa	as-cast	6.095	–	1.66	44.3	0.00	0.00	0.0
Fe_2NiGa	2w 800	5.780	–	3.21	55.0	−0.31	−0.30	5.6
Fe_2CoGa	10 d 800	5.767	–	5.09	120.9	−0.83	−0.95	6.9
Fe_2CrGa	11 d 800	5.824	–	2.60	42.5	−0.36	−0.41	8.5
Fe_2VGa	11 d 800	5.782	$\chi_g = 3\times10^{-6}$ emu/g			–	–	
Co_2FeGa	10 d 800	5.737	–	5.13	116.8	−0.82	−0.98	7.0
Co_2MnGa	10 d 800	5.767	694 (a)	4.05	87.5	−0.28	−0.31	3.2
Co_2CrGa	30 d 800	5.805	–	2.36	49.3	0.00	0.00	0.0
Co_2VGa	30 d 800	5.779	352	1.92	33.2	−0.04	−0.03	1.2
Co_2NbGa	14 d 800	5.950	–	1.39	20.9	−0.02	−0.02	1.0
Co_2TiGa	as-cast	5.850	130 (b)	0.75 (b)	–	–	–	
Co_2HfGa	as-cast	6.032 (b)	186 (b)	0.60	–	–	–	
Ni_2MnGa	8 d 900	5.835	379 (c)	4.07	69.7	0.00	0.00	0.0

Table 8
Crystalchemical, magnetic and magneto-optical data of Heusler ($L2_1$-type) compounds based on Sn. The saturation magnetization per formula unit (μ_s) was derived from magnetization measurements at 4.2 K in a field of 1440 kA/m. The magnetization (σ) and the polar Kerr rotation angle ($2\varphi_K$) were obtained at room temperature in a field of 1280 kA/m. (a) Ref. [14]

Compound	Heat treatment	a (Å)	T_C (K)	μ_s (μ_B/FU)	σ (Am^2kg^{-1})	$2\varphi_K$ (deg)		$\frac{2\lvert\varphi_K\rvert}{\sigma} \times 10^3$
						633 nm	830 nm	
Fe_2VSn	50 d 600	5.959	200	1.32	8	−0.05	0.07	0.1
Co_2TiSn	30 d 800	6.076	371	1.96	35.8	0.00	+0.01	0.0
Co_2ZrSn	20 h 900	6.242	448	1.46	–	+0.18	−0.04	–
Co_2HfSn	11 d 800	6.227	394 [a]	1.57	19.8	+0.31	0.00	15.7
Co_2VSn	14 d 800	5.960	95	1.21		+0.02	+0.01	–
Co_2NbSn	60 d 600	6.142	105	0.69		–	–	
Co_2MnSn	10 d 800	5.984	829 [a]	4.79	87.3	−0.06	−0.11	0.7
Ni_2MnSn	30 d 800	6.048	345	4.01	48	+0.01	+0.02	0.0
Cu_2MnSn	20 d 640	6.168	530	3.97	60.8	−0.12	−0.14	2.0

(Z = Al, In, Sn) are compared in fig. 12. It can be seen that these three spectra have a similar shape although the Kerr amplitude increases strongly in going from Al to Sn. In these cases it is also possible that the spectra have to be analysed in terms of charge transfer transitions between the exchange splitted 3d states of Mn and the p states of Z = Al, In or Sn. Indications in support of this interpretation are obtained from the spin–orbit splitting constant of the Z component, which is very small for Al and equal to 2.4×10^{-3} and 3.8×10^{-3} cm^{-1} in he case of In and Sn, respectively [18]. In the case of charge transfer transitions one would expect the intensity of the mag-

Table 9
Crystal chemical, magnetic and magneto-optical properties of several Heusler ($L2_1$-type) compounds based on Si, Ge and Pb. The saturation moment per formula unit (μ_s) was obtained from magnetic measurements at 4.2 K in a field of 18 kOe. The values of the magnetization (σ) and the polar Kerr rotation angle ($2\varphi_K$) were obtained at room temperature in a field of 1280 kA/m

Compound	Heat treatment	a (Å)	T_c (K)	μ_s (μ_B/FU)	σ (Am^2kg^{-1})	$2\varphi_K$ (deg)		$\frac{2\lvert\varphi_K\rvert}{\sigma} \times 10^3$
						633 nm	830 nm	
Co_2FeSi	20 d 600	5.647	980 [a]	5.18	139.8	−0.67	−0.68	4.8
Fe_2VSi	11 d 800	5.675	$\chi = 2.5 \times 10^{-5}$ g/emu		–	–	–	–
Co_2TiSi	12 d 900	5.743	375 [b]	1.65	37.3	0.00	−0.05	0.0
Fe_2MnSi	10 d 800	5.671	–	2.33	–	−0.05	−0.04	–
Co_2MnSi	30 d 800	5.645	985 [c]	4.90	138.4	0.00	−0.06	0.0
Co_2FeGe	20 d 600	5.738	–	5.54	124.2	−0.87	−1.03	7.0
Co_2MnGe	10 d 800	5.749	905 [c]	4.93	108.8	−0.03	−0.08	0.3
Co_2TiGe		5.807	386 [b]	1.59	26.6	+0.01	−0.01	0.4
Fe_2CoGe	14 d 800	5.775	–		118.2	−0.71	−0.79	6.0
Ni_2MnIn	20 d 600	6.075	323 [c]	4.34	40.3	0.00	0.00	0.0
Cu_2MnIn	20 d 520	6.206	500 [c]	3.95	64.1	−0.05	−0.03	0.8
Co_2FeIn	30 d 400	5.716	–	–	–	−0.88	−1.17	–
Rh_2MnSn	24 d 800	6.232	410 [d]	3.4 [a]	41	+0.01	+0.02	0.2
Rh_2MnGe	as-cast	6.044	–	–	27	0.00	+0.01	0.0
Rh_2MnPb	as-cast	6.271	335 [d]	2.9 [d]	3.5	0.00	0.00	0.0
Ru_2FeSn	24 d 800	6.202	–	–	33	−0.14	−0.08	4.2

[a] Ref. [14]; [b] ref. [15]; [c] ref. [16]; [d] ref. [17].

Table 10
Crystalchemical, magnetic and magneto-optical data of several Heusler compounds based on Sb an Sn. The values of the saturation magnetization (μ_s) were obtained from measurements at 4.2 K and 1440 kA/m. The values of the magnetization (σ) and the polar Kerr rotation angle ($2\varphi_K$) were obtained in 1280 kA/m at room temperature

Compound	Heat treatment	Structure	a (Å)	T_C (K)	μ_s (μ_B/FU)	σ (Am^2kg^{-1})	$2\varphi_K$ (deg)		$\frac{2\lvert\varphi_K\rvert}{\sigma} \times 10^3$
							633 nm	830 nm	
Ni_2MnSb	7 d 800 (q)	$L2_1$	5.982		3.22	37	+0.01	−0.06	0.3
Co_2MnSb	12 d 700	$L2_1$	5.917		4.52	58	−0.03	−0.13	0.5
NiMnSb	14 d 850 (q)	$C1_b$	5.920	730	3.85	90	−0.07	−0.60	0.8
CoMnSb		$C1_b$	5.875	490	3.93	85	−0.03	−0.08	0.1
RhMnSb	7 d 800 (q)	$C1_b$	6.150	320	3.81	30	+0.01	−0.04	0.3
PdMnSb	14 d 850 (q)	$C1_b$	6.285	500	3.95	53	−0.28	−0.28	5.3
PtMnSb	14 d 850 (q)	$C1_b$	6.210	585	3.97	54	−1.86	−1.53	34.4
CuMnSb	14 d 600 (q)	$C1_b$	6.095	55 (T_N)	–	–	–	–	–
$Co_{0.3}Cu_{0.7}MnSb$	11 d 700 (q)	$C1_b$	6.054		4.42		−0.12	−0.10	
$Co_{0.3}Ir_{0.8}MnSb$	11 d 700 (q)	$C1_b$	6.095		2.82		−0.03	−0.10	
$Co_{0.1}Ir_{0.9}MnSb$	11 d 700 (q)	$C1_b$					0.00	0.00	
PtFeSb	14 d 700	FO_1	6.439	493		20	−0.12	−0.13	6.0
PtCrSb	14 d 700	FO_1	6.444				–	–	–
PtMnSn	as-cast	$C1_b$	6.264	330	3.52	30	−0.29	−0.22	9.7

neto-optical transition to follow the same trend.

Record values of the Kerr intensity were observed in the compound PtMnSb [19]. As shown in more detail elsewhere, the Kerr spectrum of this compound has a strong intensity near 1.7 eV (720 nm) in excess of $2\varphi_K = 2.5°$. The compound PtMnSb has the cubic Cl_b structure which is strongly related to the $L2_1$ structure. In table 10 we present the results of several compounds which, in one way or the other, bear a resemblance to PtMnSb. It can be derived from these data that the strong Kerr intensity in PtMnSb is reduced considerably when Pt is replaced by Pd, Rh, Co or Ni, and also when Sb is replaced by Sn, even though the crystal structure remains the same.

Another type of ternary compound is that of the hexagonal Ni_2In structure. As an example fig. 13 shows the Kerr spectrum of FeCoSn. This spectrum has basically the same features as those of the parent metals Fe and Co, and the same is true of many other members of this group. Results for compounds in which this structure type was observed are listed in table 11. A more detailed account of the magnetic and magneto-optical properties of these ternaries has been given elsewhere [20]. Finally, we have listed in table 12 experimental data for the cubic ternary compounds of the $Cr_{23}C_6$ type. It can be inferred from these results that the members of this series show a rather uniform behaviour, except for the two Fe-base compounds at the bottom of the table which have relatively large $2\varphi_K$ values at the two wavelengths considered.

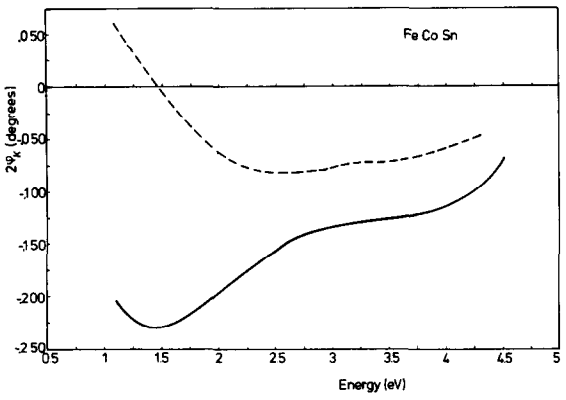

Fig. 13. Kerr spectrum of the Ni_2In type compound FeCoSn. Full line: Kerr rotation ($2\varphi_K$); broken line: ellipticity.

4. Discussion

In order to correlate the Kerr spectra with transition matrix elements it would be necessary to combine the results for the Kerr rotation and ellipticity with results for the complex dielectric constant. After computation of the off-diagonal elements of the dielectric tensor one is then able to

Table 11
Crystalchemical, magnetic and magneto-optical data of several hexagonal Ni_2In-type compounds. The values of the saturation magnetization (μ_s) were obtained at 4.2 K in a field of 1440 kA/m. The values of the magnetization (σ) and the polar Kerr rotation angle ($2\varphi_K$) were obtained at room temperature in a field of 1280 kA/m

Compound	Heat treatment	Lattice constants		μ_s (μ_B/FU)	σ (Am^2 kg^{-1})	$2\varphi_K$ (deg)		$(2\|\varphi_K\|)/(\sigma)$ $\times 10^3$
		a(Å)	c(Å)			633 nm	830 nm	
PtMnAl	6 d 800	4.336	5.501	$\chi_g = 1.7\times10^{-5}$ emu/g	–	–	–	–
PtMnGa	6d 800	4.336	5.590	3.15	–	–	–	–
FeNiIn	21 d 600	4.377	5.313	2.20	23.3	−0.25	−0.24	10.7
FeMnIn	as-cast	4.302	5.356	3.40		−0.09	−0.11	
FeNiGe	10 d 800	4.039	5.103	0.70	11	−0.08	−0.08	7.3
FeCoGe	14 d 800	4.002	5.035	2.50	43.2	−0.30	−0.30	6.9
FeMnGe	10 d 800	4.112	5.242	1.65	9.3	−0.02	−0.03	2.2
CoNiSn	as-cast	4.120	5.208	0.70	–	−0.07	−0.07	–
FeNiSn	30 d 700	4.134	5.190	1.37	28.7	−0.12	−0.14	4.2
FeCoSn	10 d 800	4.175	5.278	2.07	34.6	−0.20	−0.23	5.8
MnCoSn	10 d 800	4.280	5.394	2.21	27.0	−0.03	−0.03	1.1

Table 12
Crystalchemical, magnetic and magneto-optical data of several cubic $Cr_{23}C_6$-type compounds. The saturation moment (μ_s) was derived from magnetic measurements at 4.2 K in a field of 1440 kA/m. The values of the magnetization (σ) and the polar Kerr rotation angle ($2\varphi_K$) refer to room temperature and an external field of 1280 kA/m

Compound	Heat treatment	a (Å)	T_c (K)	μ_s (μ_B/Co)	σ (Am^2kg^{-1})	$2\varphi_K$ (deg)		$(2\|\varphi_K\|)/(\sigma)$ $\times 10^3$
						633 nm	830 nm	
$Co_{20}Al_3B_6$	30 d 800°C	10.513	409	0.57	39.5	−0.25	−0.27	6.3
$Co_{20}Ga_3B_6$	30 d 800°C	10.502	–	1.15	40.3	−0.31	−0.29	7.7
$Co_{21}Sn_2B_6$	18 d 800°C	10.604	–	0.50	50.5	−0.39	−0.39	7.7
$Co_{21}Ge_2B_6$	18 d 800°C	10.501	467	0.47	33.8	−0.22	−0.25	6.5
$Co_{21}V_2B_6$	18 d 800°C	10.486	–	0.80	57.4	−0.34	−0.29	5.9
$Co_{21}Nb_2B_6$	18 d 800°C	10.546	491	0.79	50.1	−0.30	−0.32	6.0
$Co_{21}Cr_2B_6$	as-cast	10.472	–	0.84	63.6	−0.37	−0.38	5.8
$Co_{21}Mo_2B_6$	20 d 800°C	10.498	545	0.76	53.7	−0.31	−0.32	5.8
$Co_{21}W_2B_6$	18 d 800°C	10.498	538	0.81	52.6	−0.38	−0.33	7.2
$Co_{20}Ti_3B_6$	18 d 800°C	10.549	478	0.68	46.2	−0.22	−0.21	4.8
$Co_{21}Zr_2B_6$	18 d 800°C	10.607	–	0.86	62.5	−0.41	−0.43	6.6
$Co_{21}Hf_2B_6$	18 d 800°C	10.617	–	0.93	56.8	−0.40	−0.42	7.0
$Co_{21}U_2B_6$	20 d 800°C	10.659	–	0.78	44.7	–	–	–
$Co_{21}Ta_2B_6$	as-cast	10.540	–	0.96	54.6	−0.34	−0.43	6.2
$Co_{20}In_3B_6$	11 d 800°C	10.604	–	0.60	–	−0.27	−0.32	–
$Fe_{21}Mo_2C_6$	18 d 800°C	10.546	492	1.53	98.2	−0.38	−0.42	3.9
$Fe_{21}W_2C_6$	18 d 800°C	10.533	1006	1.42	97.4	−0.69	−0.74	7.1
$Fe_{23}C_3B_3$	as-cast	10.627	742	1.98	178.5	−0.75	−0.86	4.2

band transitions. Since results of measurements of the wavenumber dependence of the complex dielectric constant are in general not available, the interpretation of the spectra given below has to be regarded as tentative.

Erskine and Stern [21] showed that the two φ_K maxima occurring in the Kerr spectrum of Ni near 1.5 and 3.2 eV are due to d–p transitions involving the d electrons at the top of the majority spin band and at the bottom of the minority spin band, respectively. The results shown in fig. 1 for the Ni alloys indicate that the transition at 3.2 eV becomes reduced in relative intensity and shifts to lower energies when Ni is alloyed with s, p elements like Al, Sn and In. A possible explanation is that the hybridization between p electrons and 3d electrons affects primarily the states at the bottom of the 3d band. It was mentioned in section 3.1 that a different behaviour is observed when Ni is alloyed with Pd and Pt. The smearing-out of the second transition towards higher energies may be due to a change of the 3d band shape near the bottom of the band, but it can equally well be the result of transitions involving the 4d or 5d electron bands which have become spin-polarized by the Ni moments. In that case it would be understandable that the shift to higher energy is larger with Pt, because the Pt d levels are expected to have a lower energy than those of Pd, Pt being the more noble material.

According to Erskine and Stern [21] the Kerr spectra of Ni and Co are similar enough to associate the same type of transition with the two φ_K maxima observed at 1.4 and 3.9 eV in the latter metal. Pushing this similarity a little further, the Kerr spectra shown for Co-base materials in figs. 3–6 can be interpreted in the same way as for the Ni-base alloys: the shift of the second peak and its reduction in intensity upon alloying with s, p metals may again be due to a strong hybridization at the bottom of the 3d band. The results shown for Co–Pd and Co–Pt alloys in figs. 5 and 6 indicate that the transition near 3.2 eV becomes enhanced in intensity relative to the transition at lower energies. This enhancement increases with increasing Pd or Pt concentration. Note that the intensity of the second maximum in $Co_{0.25}Pt_{0.75}$ has become twice as strong as the first maximum.

These results strongly suggest that the additional intensity in the 4 eV region is associated with transitions from the 4d or 5d band. Moreover, the second maximum occurs at higher energy in the Pt alloys than in the Pd alloys. We have already discussed this feature when dealing with alloys of Pd and Pt with Ni. It is easy to show that the 4d or 5d bands have become spin-polarized by the Co moments. For instance in fcc PtCo we observed a saturation moment at 4.2 K equal to $2.05\mu_B$ per formula unit. This is appreciably higher than the $1.7\mu_B$ observed for the moment per Co atom in Co metal. Evidently the Pt atoms contribute a moment equal to $0.35\mu_B$/Pt. The relatively strong contribution of the transitions involving 4d or 5d electrons, in spite of the moment being lower than the 3d moment, is very likely a result of the larger spin–orbit splitting associated with the 4d and 5d electrons. This would also explain why the enhancement is larger in Co–Pt alloys (where the Kerr rotation near 4 eV considerably exceeds that of pure Co) than in Co–Pd alloys because the spin–orbit splitting in Pt is much higher than in Pd [22]. Accordingly, the high energy peak in $Ni_{92}Pt_8$ is also enhanced and is larger than in the Ni–Pd alloy.

For the Fe-base materials this type of interpretation is less easily made because the second transition in the Kerr spectra is less sharp and also involves energies outside the range considered in this investigation. From the general behaviour of the spectra it would seem, however, that the trends are the same as in Ni- and Co-base materials. The variety of different spectra of Mn-base materials on the other hand suggests that the situation here is much more complex.

Inspection of the spectra of the materials based on Ni, Co or Fe shows that the position of the first φ_K maximum is relatively stable, except for alloys in which the concentration of the non-magnetic component is relatively high. This first φ_K maximum is associated with transitions from the top of the majority 3d band and its intensity is a measure of the strength of the 3d band splitting. This feature can be used to investigate whether one may expect a correlation between the 3d moment size (or the magnetization) and the Kerr rotation measured in this energy range. For Co-base materials we have compared the concentration dependence of $2\varphi_K$ measured at $\lambda = 633$ nm (2 eV) with the corresponding magnetization σ in figs. 14–17. The broken line in these plots represents the reduced Kerr rotation defined as the ratio $2\varphi_K/\sigma$.

A relationship between φ_K and σ exists in all systems, though in most cases the Kerr rotation is not proportional to the magnetization. Here the effective Kerr rotation increases significantly with decreasing Co content. In the $Pt_{1-x}Co_x$ and $Ir_{1-x}Co_x$ system we ascribe this effect mainly to the increasing participation of the 5d electrons with their large spin–orbit coupling. In the other systems the reason for the increase of the reduced Kerr rotation is still unclear, although it might be associated with the observation that it occurs predominantly at concentrations where the room temperature magnetization has a tendency to vanish. This may, for instance, indicate a correlation between the Kerr effect and a possible change from strong ferromagnetism (only one spin band partially depleted) to weak ferromagnetism (both spin bands partially depleted) preceding the magnetic collapse.

Similar plots as described above for the Co-base materials have also been made for Fe-base materials. These plots are displayed in figs. 18–20. Using the same arguments as in the case of Co-base materials one may again speak of a reasonably strong correlation between $2\varphi_K$ and σ. The strong increase with decreasing x of the reduced Kerr rotation $2\varphi_K/\sigma$ in $Pt_{1-x}Fe_x$ is again ascribed to

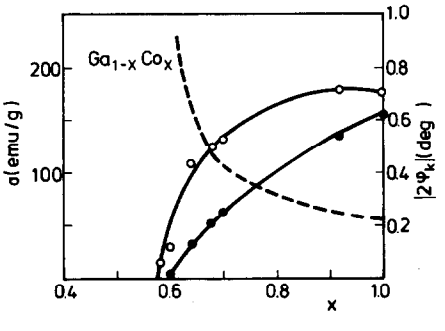

Fig. 14. Concentration dependence of the Kerr rotation ($2\varphi_K$; open circles) and the room temperature magnetization (σ; full circles) in $Ga_{1-x}Co_x$. The reduced Kerr rotation (arb. scale) is indicated by the broken line.

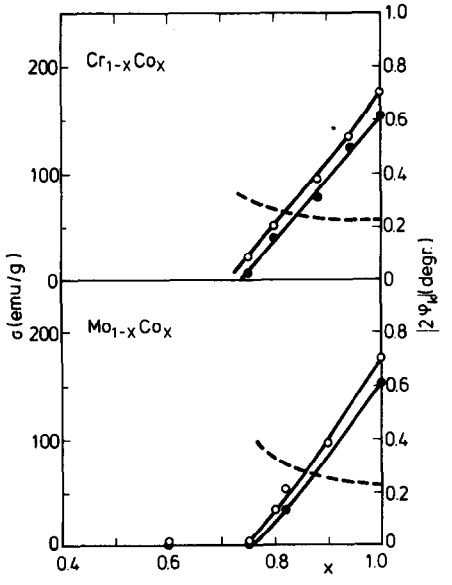

Fig. 15. Concentration dependence of the Kerr rotation at $\lambda = 633$ nm ($2\varphi_K$; open circles) and the room temperature magnetization (σ; full circles) in $Cr_{1-x}Co_x$ and $Mo_{1-x}Co_x$. The concentration dependence of the reduced Kerr rotation is indicated by broken lines.

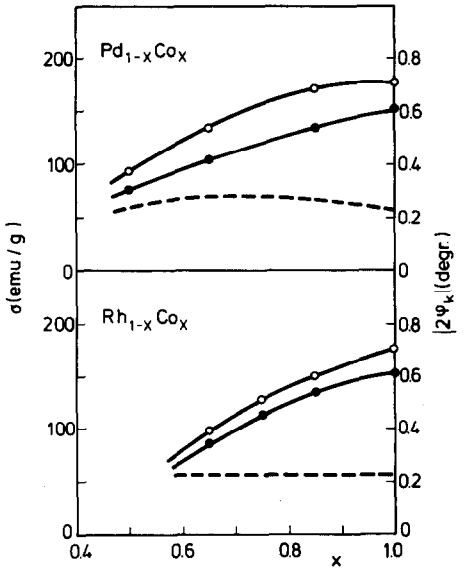

Fig. 16. Concentration dependence of the Kerr rotation at $\lambda = 633$ nm ($2\varphi_K$; open circles) and the room temperature magnetization (σ; full circles) in $Pd_{1-x}Co_x$ and $Rh_{1-x}Co_x$. The concentration dependence of the reduced Kerr rotation is indicated by broken lines (in arbitrary units).

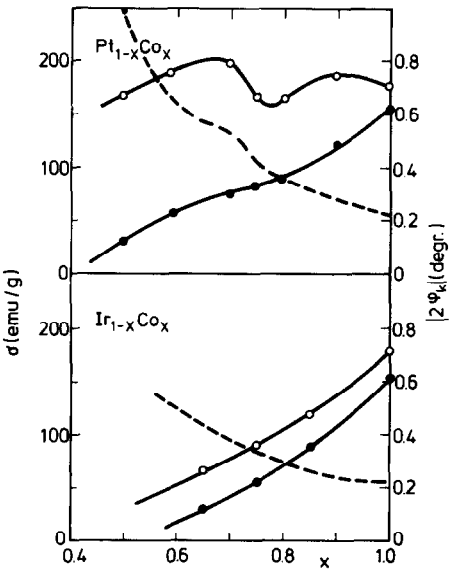

Fig. 17. Concentration dependence of the Kerr rotation at $\lambda = 633$ nm ($2\varphi_K$; open circles) and the room temperature magnetization (σ; full circles) in $Pt_{1-x}Co_x$ and $Ir_{1-x}Co_x$. The concentration dependence of the reduced Kerr rotation is indicated by broken lines (in arbitrary units).

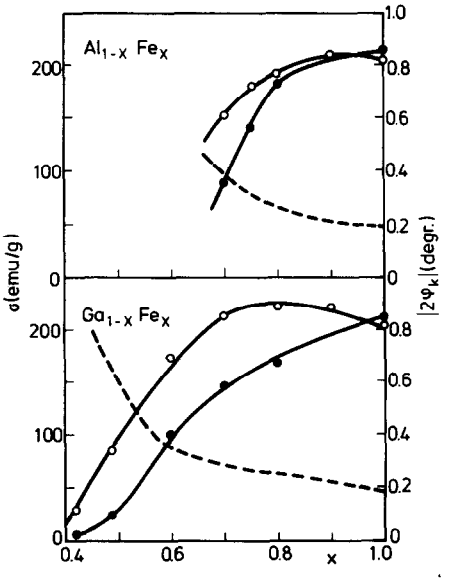

Fig. 18. Concentration dependence of the Kerr rotation at $\lambda = 633$ nm ($2\varphi_K$; open circles) and the room temperature magnetization (σ; full circles) in $Al_{1-x}Fe_x$ and $Ga_{1-x}Fe_x$.

compare these values with the various possible the increasing effect of the 5d electrons of Pt on the magneto-optical spectra. It was already pointed out in section 3.1 that the concentration dependence of $2\varphi_K$ and σ is less easily studied in the Ni-base materials owing to the absence of magnetic Ni compounds. Note that here too there is a relatively large effective Kerr rotation in the case of X = Pt.

Summarizing the results of this investigation, we can say that we did not find experimental evidence for the often intuitively adopted assumption that the Kerr rotation in magnetic metal systems is proportional to the magnetization. This

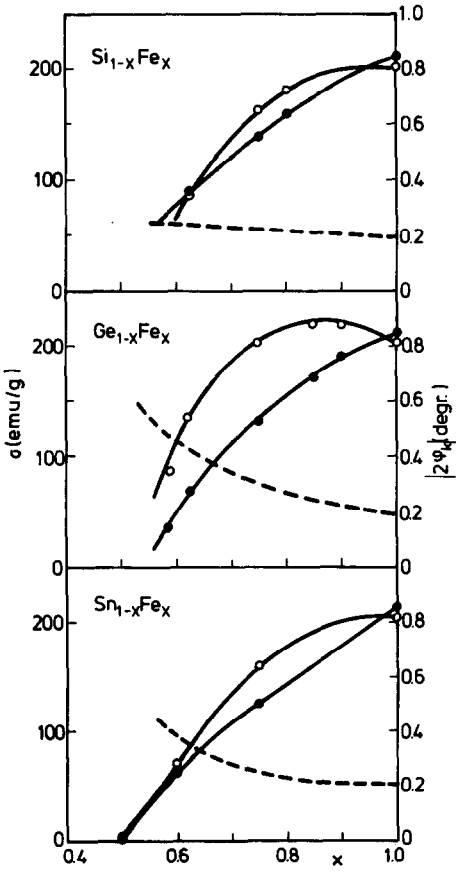

Fig. 19. Concentration dependence of the Kerr rotation at $\lambda = 633$ nm ($2\varphi_K$; open circles) and the room temperature magnetization (σ; full circles) in Si–Fe, Ge–Fe and Sn–Fe alloys and compounds. The broken line represents the concentration dependence of $2\varphi_K/\sigma$ (in arbitrary units).

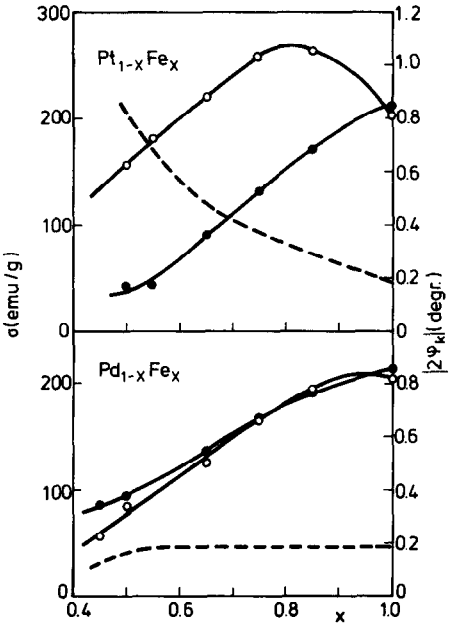

Fig. 20. Concentration dependence of the Kerr rotation at $\lambda = 633$ nm ($2\varphi_K$; open circles) and the room temperature magnetization (σ; full circles) in $Pt_{1-x}Fe_x$ and $Pd_{1-x}Fe_x$. The broken line represents the concentration dependence of $2\varphi_K/\sigma$ (in arbitrary units).

holds for Mn-base materials in particular, but it also holds for a large number of the materials based on the remainder of magnetic 3d metals. Only when the Fe or Co concentrations are fairly high can one speak of an approximately linear relationship between the Kerr rotation and the corresponding magnetization. In this high concentration limit the magnetization can serve as a guide in efforts to find multicomponent metal systems, not considered in this study, that have sufficiently high $2\varphi_K$ values. Speaking again of Fe- and Co-base materials, the concentration regions (lower than 70at% 3d metal) where severe deviations (in a positive sense) from the ratio $2\varphi_K/\sigma$ occur, are unfortunately not interesting from the viewpoint of practical magneto-optical applications since here the $2\varphi_K$ values are small compared to those in the parent 3d metals, the only exception being Pt alloys. From the systematic behaviour found in Co- and Fe-base materials it may also be predicted that at practical wave-

lengths (He–Ne laser or GaAs laser) the Kerr rotation $2\varphi_K$ will be restricted to the range $2\varphi_K \lesssim 1°$ in metallic systems where the magnetic properties are determined by Fe or Co. Furthermore the Kerr rotations in Ni-base metallic systems are too small for magneto-optical applications.

In Mn-base materials we did not even find a correlation between the Kerr rotation and the magnetization. However, it is this very class of materials that comprises the compounds PtMnSb and MnBi which have recorded Kerr effect values [19,23,24]. In the further search for better magneto-optical metal systems, those based on Mn seem the most promising ones.

Acknowledgements

The authors are indebted to W.W. van den Hoogenhof for his experimental assistance in the magnetic measurements and to P. Hokkeling and H.T. Munsters for their help in the preparation of the samples.

References

[1] K. Lee, J. Vac. Sci. Techn. 10 (1973) 631.
[2] P. Dekker, IEEE Trans. Magn. MAG-12 (1966) 311.
[3] D. Treves, J.T. Jacobs and E. Sawatzky, J. Appl. Phys. 46 (1975) 2260.
[4] P. Chaudhari, J.H. Cuomo and R.J. Gambino, IBM J. Res. Develop. 11 (1973) 66.
[5] H. Heitmann, I. Sander, M. Urner-Wille and K Witter, J. Magn. Magn. Mat. 21 (1980) 233.
[6] Y. Togami, IEEE Trans. Magn. MAG-18 (1982) 1233.
[7] K.A. Schouhamer Immink and J.J.M. Braat, to be published.
[8] C.J. Smithells, Metals. Reference Book, 5th ed. (Butterworths, London, 1976).
[9] R.P. Elliot, Constitution of Binary Alloys, First Suppl. (McGraw-Hill, New York, 1965).
[10] F.A. Shunk, Constitution of Binary Alloys, Second Suppl. (McGraw-Hill, New York, 1969).
[11] J.H. Wernick, S.E. Hazko and W.J. Romanov, J. Appl. Phys. 32 (1961) 2495.
[12] K.H.J. Buschow and P.G. van Engen, J. Magn. Magn. Mat. 25 (1981) 90.
[13] P.G. van Engen, K.H.J. Buschow and M. Erman, J. Magn. Magn. Mat. 30 (1983) 374.
[14] V. Niculescu, T.J. Burch, K. Raj and J.I. Budnick, J. Magn. Magn. Mat. 5 (1977) 60.
[15] P.J. Webster and K.R.A. Ziebeck, J. Phys. Chem. Solids 34 (1973) 1674.
[16] C.C.M. Campbell, J. Phys. F5 (1975) 1931.
[17] S.R. Dhar, A.K. Grover, S.K. Malik and R. Vijayaraghavan, Solid State Commun. 33 (1980) 545.
[18] C.K. Jorgensen, Orbitals in Atoms and Molecules (Academic Press, London, 1962).
[19] P.G. van Engen, K.H.J. Buschow, R. Jongebreur and M. Erman, Appl. Phys. Lett. 42 (1983) 202.
[20] K.H.J. Buschow and P.G. van Engen, Phys. Stat. Sol. (a) 76 (1983) in press.
[21] J.L. Erskine and E.A. Stern, Phys. Rev. Lett. 30 (1973) 1329.
[22] J.S. Griffith, The Theory of Transition Metal Ions (Cambridge Univ. Press, Cambridge, 1961).
[23] K. Egashira and T. Yamada, J. Appl. Phys. 45 (1974) 3643.